# Antireflection Surfaces Prepared from Fluorinated Latex Particles

**Jong-Wook Ha,* In Jun Park, and Soo-Bok Lee**

*Biorefinery Research Center, Korea Research Institute of Chemical Technology, Daejeon 305-343, Korea*

*Received June 2, 2008; Revised Manuscript Received September 25, 2008*

ABSTRACT: We prepared porous antireflection surfaces from spin-coating of poly(2,2,2-trifluoroethyl methacrylate) (PTFEMA) latex particles onto bare glass slides. Optical properties resulting from two different coating structures, multilayer and submonolayer of latex particles, were studied depending upon the particle size. In both cases, the characteristic matrix theory based on the classical Fresnel coefficient of reflection applied to estimate the effective refractive index and thickness of the porous coatings from experimentally measured reflectance spectra. The particle fraction in the coatings was estimated by using a volume-averaged refractive index. For porous multilayer coatings prepared from 47 nm PTFEMA latex particles, it was found that the effective refractive indices ($n_{eff} \sim 1.34$) and reflectance minima ($R_{min} \sim 0.7\%$) were almost constant and independent of the coating thickness. On the other hand, the effective refractive indices were strongly dependent on the coating conditions in the case of submonolayer coatings of 140 nm PTFEMA latex particles. As increasing the solid content of the coating solutions or, equivalently, as increasing the particle fraction in the coatings, the effective refractive indices increased. The minimum specular reflectance was as low as 0.2% when the particle volume fraction in the coating was 0.40.

## Introduction

Reduction or elimination of unwanted light reflection and glare and increase of light transmission have been received much attention for nearly two centuries in order to improve the performance of optical components made from glass-based materials. As a result, many sophisticated techniques based on the deposition of inorganic precursors have been developed and successfully applied to commercial processes, for example, single-layer interference coatings, two-layer V-coatings, and multilayer broadband antireflection coatings. At the same time, the demand for antireflection coating technology applicable to polymeric substrates independent of their shape and size is increasing due to the rapid growth of flat panel display industries. To this end, it is still required to develop simple, economic, and environmentally benign methods which are appropriate for roll-to-roll processes.

The fundamental principle of single-layer antireflection coatings is well understood. In brief, a thin film of transparent dielectric is coated on the substrate so that the reflections of light from the outer surface of the film and the film−substrate interface cancel each other by destructive interference.[1] The reflected beams can be canceled with a single-layer coating only if the reflections are exactly 180° ($\pi$ radian) out of phase and they have the same intensity. These conditions are related to the thickness and refractive index of the coating, respectively. If the optical thickness of the coating is identical to a quarter of the desired wavelength, the reflections are in a condition of exact destructive interference. In addition, the refractive index ratio must be the same at both the interfaces in order that the two reflected beams have equal intensities. If it is assumed that the light travels through the air, the coating should have ideally a refractive index of $n_c = \sqrt{n_s}$, in which $n_c$ and $n_s$ stand for the refractive indices of the coating and substrate, respectively. For example, it is required for complete elimination of light reflection at a certain wavelength that the refractive index of coating is equal to 1.23 when the glass ($n_s = 1.52$) is used as a substrate.

* To whom correspondence should be addressed. E-mail: jongwook@krict.re.kr.

Although suitable materials that can be utilized in the fabrication of homogeneous films with such a low refractive index and durability have not been reported yet, it is possible to reach an effective refractive index satisfying the above-mentioned requirements with porous dielectric materials. The pore size must be much smaller than the electromagnetic wavelengths of interest in this case. One of the traditional methods is to etch the substrate by using chemicals or laser ablation, resulting in a roughened, porous surface layer.[2,3] Recently, with the progress of vacuum-related technologies, sputtering, physical vapor deposition, and plasma-enhanced chemical vapor deposition have been widely used to produce porous layers onto various substrates including plastics.[4−8] It has been also carried out to fabricate microscopically porous coatings from a single or multiple wet processes. After phase separation of block copolymer or polymer blend films coated on the substrate, one of the phases is selectively removed by solvent to leave porous polymer films with good antireflection properties.[9,10] The so-called porogen generating pores in the coatings during the process is frequently used to produce inorganic or polymeric porous films from sol−gel or polymer solutions.[11−14] Electrostatic layer-by-layer deposition of oppositely charged polyelectrolytes or inorganic particles under the precise control of coating conditions can be used to produce tunable antireflection films.[15−20] The porous coatings fabricated from colloidal particles with appropriate size have been found to effectively reduce the light reflection of substrates. The charged particles are deposited on the glass substrates pretreated with polyelectrolyte multilayer in conventional,[21,22] but much more convenient and simple methods have been proposed more recently for deposition of inorganic or polymeric particles utilizing convective assembly or spin-coating.[23−27] It has been also reported that the colloidal particles can be used as template for the fabrication of biomimic antireflection surfaces.[28−30]

In this study, we examine the antireflective properties of porous coatings fabricated from fluorinated latex particles on bare glass substrates. Fluorinated polymers have occupied an important position in material science and have been used in many industrial fields, mainly due to their excellent mechanical properties such as heat resistance and chemical inertness.[31−33] Besides conventional applications, it has been found that unique

10.1021/ma801224w CCC: $40.75 
Published on Web 10/22/2008

properties of fluorinated polymers such as low surface energy, low friction coefficient, and low refractive index are very useful in a myriad of emerging technologies. Amorphous fluorinated polymers, for example, are successfully applied in plastic fiber optics and antireflection films where the low refractive index is a crucial factor. Since these properties cannot be obtained from other materials based on hydrocarbon or silicone compounds, the interest in the fluorinated polymers is enlarging. In the following sections, experimental details and optical properties of submonolayer and multilayer porous coatings prepared from spin-coated poly(2,2,2-trifluoroethyl methacrylate) (PTFEMA) latex particles are reported.

## Experimental Section

**Materials and Particle Preparation.** The fluorinated latex particles were synthesized by conventional emulsion polymerizations of partially fluorinated monomer, 2,2,2-trifluoroethyl methacrylate (TFEMA, Tosoh F-Tech, Inc). For the synthesis of the smaller (47 nm) PTFEMA latex particles, 4.5 g of TFEMA and 0.5 g of ethylene glycol dimethacrylate (EGDMA, Aldrich) were mixed and emulsified in 56.5 g of deionized water dissolving 1.5 g of anionic surfactant, sodium lauryl sulfate (SLS, Acros) by ultrasonic during 10 min. The emulsified mixture was transferred into 3-neck flask equipped with mechanical stirrer and thermocouple. When the temperature inside the reactor reached to 70 °C in an oil bath, 0.3 g of sodium persulfate (SPS, Aldrich) dissolved in 2 g of deionized water was injected into the flask to initiate the polymerization. Remaining monomers, 49.5 g of TFEMA and 5.5 g of EGDMA, were emulsified in 65 g of water containing 1.5 g of SLS by ultrasonic and fed into the reactor continuously via precision metering pump as a rate of 30 mL/h after 30 min of seed formation step. The polymerization lasted for 3 h after completing monomer addition. The polymerized product was filtered through glass wool to remove little coagulum. The solid content of final product was 33.6 wt %. The particle size was measured by photon correlation spectrometer (Zetasizer 3000HS, Malvern Instrument Inc.).

The larger (140 nm) PTFEMA latex particles were prepared from batch emulsion polymerization in three-neck flask at 70 °C. 60 g of TFEMA and 3 g of EGDMA were mixed and emulsified in 237 g of deionized water containing 0.1 g of sodium dodecyl benzoic sulfonate (SDBS, TCI) as an anionic surfactant and 0.4 g of sodium bicarbonate (SBC, DC Chemical Co., Ltd.) as a pH buffer. The polymerization was started by adding 0.3 g of SPS dissolved in 3 g of deionized water into the reactor and lasted for 6 h. The final product had 20.1 wt % solids after filtration.

In order to observe the optical properties of PTFEMA homogeneous films, TFEMA was polymerized in 2-butanone (Oriental Chemical industries). 30 g of TFEMA and 0.3 g of 2,2′-azobis(isobutyronitrile) (AIBN, Junsei) were added to 70 g of solvent. The polymerization lasted for 24 h at 65 °C. The crude polymerized product was purified by precipitation in anhydrous ethyl alcohol (Burdick & Jackson) twice and dried under reduced pressure. Finally, 27.1 g of glassy polymer was obtained. All reagents were used as received without further purification.

**Coating Characterizations.** A precleaned microscope glass slide (S-1111, Matsunami Glass Ind., Ltd.) was used as a substrate. The slides were cut into approximately 25 × 25 mm squares and cleaned by an Alconox solution (Godax Laboratories) for a minimum of several hours within ultrasonic bath. The slides were rinsed with deionized water and acetone and dried at 70 °C in convection oven. The stock emulsion products were diluted with deionized water to desired particle concentrations. The PTFEMA latex particles were spin-coated on the substrate with a rotating speed of 5000 rpm for 60 s. 200 $\mu$L of aqueous dispersion was deployed on the substrate before rotation. The coatings were dried at room temperature under atmospheric condition more than 1 day. To eliminate the backside reflection of the glass substrate, the other side of glass was painted in black. The homogeneous PTFEMA thin films were prepared similarly, except that the polymer was dissolved in 2-butanone. Reflectance of glass slides coated by PTFEMA particles or homogeneous films was measured using a UV/vis spectrophotometer (JASCO V550, Jasco Corp.) over the spectral range of 400−800 nm in specular reflectance mode with an incidence angle of 5°. Every reflectance spectrum shown below is an average of nine measurements obtained from nine different samples prepared under the same coating conditions. The surface and cross section of the coatings were observed with a field-emission scanning electron microscope (JEOL, F6400). The thickness and effective refractive index of coatings were estimated from the characteristic matrix theory based on the Fresnel coefficient of reflectance by fitting experimentally measured reflectance spectra.

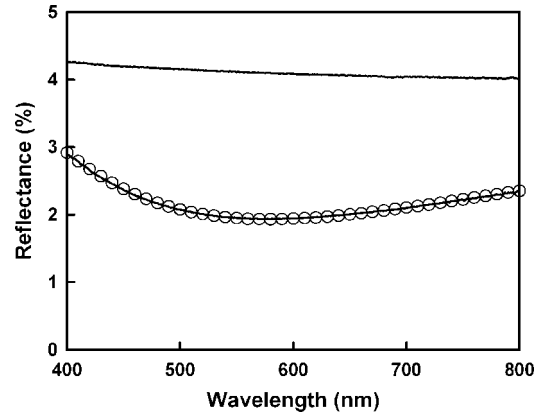


**Figure 1.** Reflectance spectrum of glass slide coated with homogeneous PTFEMA film. The PTFEMA thin film was prepared by spin-coating of 2.25 wt % solution in 2-butaneone with rotating speed of 3000 rpm for 30 s. The reflectance predicted by eq 1 is given as circles. For reference, the reflectance of bare glass slide is also included.

## Results and Discussion

**Homogeneous PTFEMA Thin Film Coatings.** Whether the single-layer antireflection coating is homogeneous or porous, the reflectance of the surface can be modeled by the Fresnel coefficient of reflection. For a thin film coating of thickness $h$ on a transparent substance, the reflectance, $R$, is given as follows:

$$R = |r|^2 = \frac{n_c^2(n_0 - n_s)^2 \cos^2 kh + (n_s - n_c^2)^2 \sin^2 kh}{n_c^2(n_0 + n_s)^2 \cos^2 kh + (n_s + n_c^2)^2 \sin^2 kh} \quad (1)$$

where $k = 2\pi n_c \cos\theta/\lambda$ is the reciprocal space number, $n_0$ is the refractive index of medium, and $\theta$ is an incidence angle of light. The refractive index and thickness of coating can be estimated accurately from eq 1 by fitting experimentally measured reflectance spectrum.

As an example, Figure 1 shows the specular reflectance of glass coated with homogeneous, nonporous PTFEMA thin film prepared from 2-butaneone solution. Because PTFEMA has lower refractive index than glass substrate, the reflectance reduced to some extent compared with the bare glass slide. The minimum reflectance was 1.94% at 570 nm, and ~50% of light reflection was diminished in visible wavelength region. By letting the refractive index and thickness of coating as two fitting parameters, the measured reflectance spectrum can be matched with calculated one, which is shown as circles in Figure 1. The refractive index and thickness of PTFEMA film estimated by eq 1 were 1.418 and 102 nm, respectively. The validity of eq 1 has been proven by many researchers mainly comparing predicted coating thickness with measured one characterized by various methods such as ellipsometry, profilometry, and atomic force microscopy after scratching the film.[10,12,23] The estimated refractive index coincides well with the reported values in the literature, which are usually around 1.42. As shown in Figure S1 in the Supporting Information, the estimated

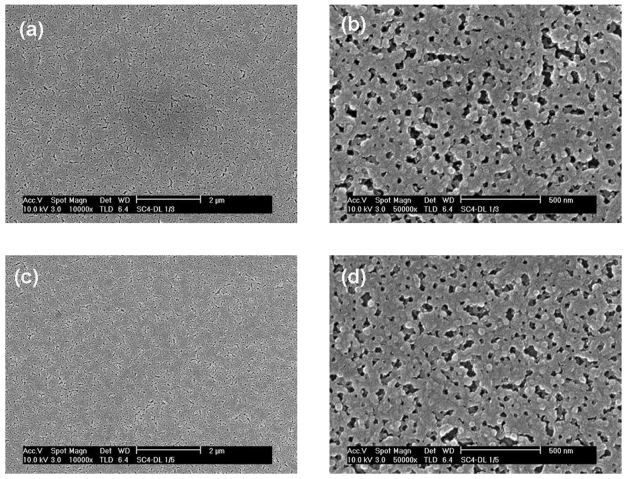


**Figure 2.** Top-down scanning electron micrographs of multilayer coatings prepared from 47 nm PTFEMA latex particle dispersions. The solid content of the coating solutions and the magnification were (a) 10.5 wt %, 10 000×; (b) 10.5 wt %, 50 000×; (c) 6.3 wt %, 10 000×; and (d) 6.3 wt %, 50 000×.

refractive indices of homogeneous PTFEMA films were almost constant to 1.42 while the film thicknesses varied from 85 to 195 nm depending on the concentration of coating solutions. This might be another evidence for the validity of eq 1 for single-layer films.

**Multilayer Porous PTFEMA Particle Coatings.** While utilizing existing materials, the refractive index of the coatings can be lowered further by introducing pores, provided that the pore sizes are much smaller than the electromagnetic wavelengths of interest. If the coating is a porous thin film constituting of particles of a few tens nanometers in diameter, the effective refractive index of the coating, $n_{eff}$, can be estimated by a volume-averaged

$$n_c^2 = n_{eff}^2 = \phi_p n_p^2 + (1 - \phi_p) n_a^2 \quad (2)$$

or the Lorentz−Lorenz relationship

$$\frac{n_{eff}^2 - 1}{n_{eff}^2 + 2} = \phi_p \frac{n_p^2 - 1}{n_p^2 + 2} \quad (3)$$

or many other relationships.[34,35] Here $\phi_p$ is the volume fraction of the particles in the coating and $n_p$ is the refractive index of the particles. There is an implicit restriction imposed on the maximal particle diameter ($d_p \ll \lambda$) in order to prevent transmission losses due to scattering. Both relations show that the effective refractive index decreases as increasing porosity or, equivalently, as decreasing the volume fraction of the particles in the coating. In principle, there is no limitation in the selection of the material constituting the particles because it is possible to control the effective refractive index arbitrarily by adjusting the volume fraction of the particles in the coating. For instance, the optimal volume fraction of particles is 0.336 for polystyrene nanoparticles ($n_p = 1.59$), while it is 0.505 for PTFEMA particles ($n_p = 1.42$) to fabricate porous thin films with $n_{eff} = 1.23$. Upon increasing the refractive index of particles, the optimal volume fraction of the particles in the coating should be decreased to match the zero reflectance condition.

The antireflective properties of porous films prepared from 47 nm PTFEMA latex particles were investigated first. The typical images of PTFEMA latex particles coated on the glass are shown in Figure 2. It is obvious that the submicron size pores are abundant and uniformly distributed over the surface.

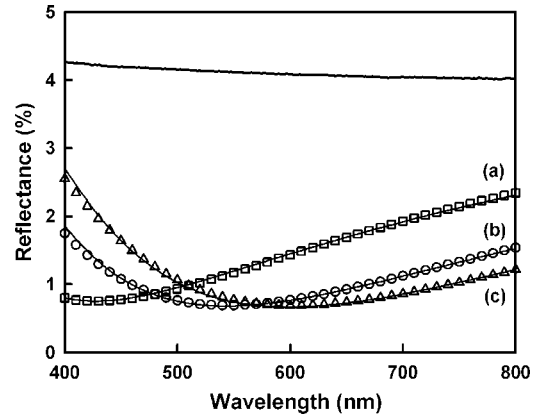


**Figure 3.** Reflectance spectra for glass slides coated with 47 nm PTFEMA latex particles. Predicted reflectance spectra are represented as open symbols. The solid content of the coating solutions were (a) 5.3, (b) 6.3, and (c) 7.9 wt %.

The uniformity of the coatings is preserved in large area without cracks or other defects. Furthermore, the surface morphology is actually independent of the solid content of the coating solutions even in the higher magnification images. The formation of pores between the latex particles can be attributed to the fact that the minimum film forming temperature of PTFEMA latex particles is higher than the ambient temperature at which the coating was carried out. The interparticle void spaces can be erased by annealing above the minimum film forming temperature because the particles deform and eventually coalesce to form a homogeneous latex film in that condition. Even though the PTFEMA particles used in this study were cross-linked slightly, it was observed the heat treatment at high temperature resulted in slight deterioration of antireflective properties, probably due to the decrease of porosity in the coatings. The use of highly cross-linked polymer particles or inorganic particles such as silica can alleviate this poor temperature response by preventing the necking between the particles and preserving more void space.

The porous thin films produced via spin-coating of PTFEMA latex particles were transparent. In other words, severe scattering or opacity was not observed due to the small size of constituent particles as well as submicron interparticle pores. Visually, changes in solid content of coating solution resulted in changes in the coloration of the light reflected off the coating, ranging from a blue tint to a yellowish tint as the solid content of coating solution increased. The reflectance minima shown in Figure 3 shifted from 430 to 620 nm, which roughly correspond to the blue, green, and yellow color sequence. The large area uniformity of the coatings was also confirmed by the fact that the reproducibility of the reflectance measurements from place to place within a sample and from one sample to another was tolerable as judged from the coefficient of variations of reflectance spectra (Figure S2 in Supporting Information).

It is noteworthy that reflectance minima shown in Figure 3 are almost identical independent of the solid content of coating solutions ($R_{min} \sim 0.7\%$). It means that the only effect of the increasing the solid content of coating solutions is increasing film thickness, but the effective refractive indices of the coatings are constant. Thus, we can conceive that the porosity in the latex films does not change with coating thickness. Again, the experimentally measured reflectance spectra can be matched with theoretical ones. Therefore, the film thickness and the effect refractive index and consequently the volume fraction of the particles in the coatings can be estimated.

While the coating thickness increased linearly with the solid content of PTFEMA particles in coating solutions, the effective

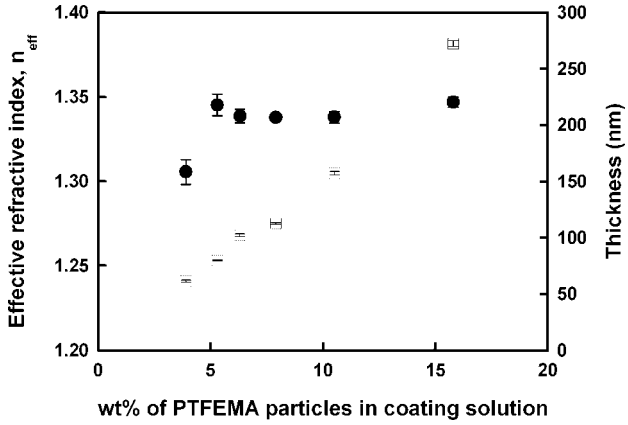


**Figure 4.** Effective refractive indices (solid circles) and coating thicknesses (open squares) estimated from eq 1 by fitting measured reflectance spectra for multilayer porous coatings of 47 nm PTFEMA particles.

refractive indices of the coatings were almost the same, except one example prepared from the coating solution with the lowest solid content as shown in Figure 4. In this case, the coating thickness estimated from eq 1 was very close to the diameter of single particle. According to the SEM image of cross-sectional area of this sample, the coating was composed of one or two layers of PTFEMA particles. It can be interpreted as an intermediate state that the coating structure is changed from submonolayer to multilayer. It is known that the packing fraction of spherical particles increases as the number of layers increases from monolayer to multilayer. The particle volume fractions and thickness of multilayer coatings with different number of particle layers and symmetry have been described by Pansu et al.[36,37] and Prevo et al.[38] Although the effective refractive index was quite low ($n_{eff} = 1.31$), the resulting optical properties was not satisfactory because the coating was too thin compared with the quarter wavelength thickness. The antireflective efficiency in visible region is diminished in this case. The effective refractive indices increased as the coating structure changed to multilayer but became constant ($n_{eff} \approx 1.34$) even though the number of particle layer and thus the coating thickness increased. This is consistent with the fact that the reflectance minima observed in Figure 3 were independent of the solid content of coating solutions. We can also speculate that the microstructure of multilayer porous films were uniform along the thickness direction.

The antireflective properties of multilayer porous particle coatings prepared from convective assembly of silica nanoparticles have been reported recently.[23] The overall structure of the coating was not much different from those observed in the present study. The polydispersity of the silica particles resulted in random close-packed structure with little long-range ordering. The particle volume fraction was centered at 0.70, and the minimum reflectance of that coating was as low as 1% for single-side reflection of glass. In our experiments, the volume fraction of the PTFEMA latex particles was 0.78 and 0.83, which were estimated from eqs 2 and 3, respectively. These values are exceeding the limit, $\phi_p = 0.74$, for three-dimensionally close-packed hard spheres. The higher particle volume fraction observed in this study can be attributed to the deformability of the latex particles, in contrast to nondeformable inorganic particles.

**Submonolayer PTFEMA Particle Coatings.** Although it has been shown that porous multilayer PTFEMA particle coatings are effective to reduce the light reflection, another strategy has to be sought in case that much better antireflection performance is required. This is due to that the effective refractive index

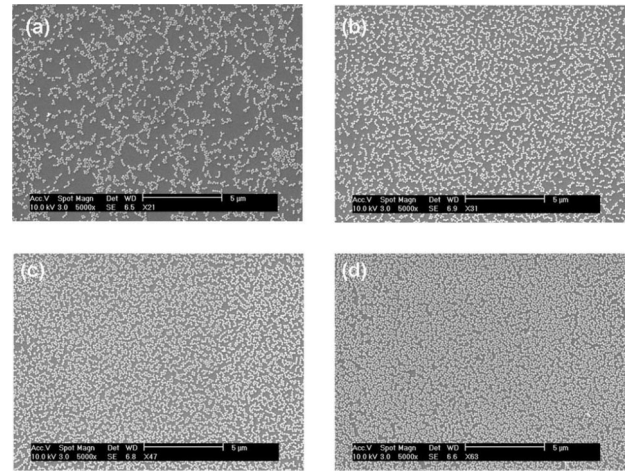


**Figure 5.** Top-down scanning electron micrographs of submonolayer coatings prepared from 140 nm PTFEMA latex particles. The solid content of the particles in coating solutions was (a) 2.1, (b) 3.1, (c) 4.7, and (d) 6.3 wt %.

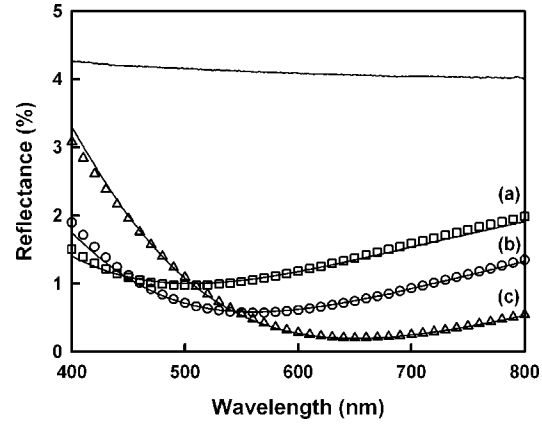


**Figure 6.** Reflectance spectra of glass slides coated with submonolayer of 140 nm PTFEMA latex particles. Reflectance spectra predicted by eq 1 are given as open symbols. For reference, the reflectance of bare glass slide is also included. The solid content of the coating solutions was (a) 2.7, (b) 3.8, and (c) 6.3 wt %.

cannot be easily controlled by varying coating conditions when the particles are packed closely in multilayer coatings as described in the previous section. In this study, we tried to fabricate the submonolayer or monolayer of much larger 140 nm PTFEMA particles in which much lower effective refractive index is expected.

Figure 5 shows the electron microscope images of the glass slides spin-coated with 140 nm PTFEMA particles. Obviously, the submonolayer of PTFEMA particles was produced, and the surface coverage by the particles was dependent upon the solid content of the coating solutions. The coating was quite uniform in large area with little ordered structure and optically transparent in spite that the larger PTFEMA particles were used.

The corresponding specular reflectance spectra are shown in Figure 6. It is evident that the reflectance minima as well as the wavelengths at the minimum reflection are varied simultaneously, which is different from the multilayer coatings discussed previously. Upon increasing the particle concentration in the coating solutions and, consequently, increasing the surface coverage by the particles, the minimum reflectance decreased while the wavelength at minimum reflectance increased. The minimum reflectance reached to 0.2%, and further reduction of reflectance was also possible with precise control of the coating condition such as rotating speed (Figure S3 in Supporting

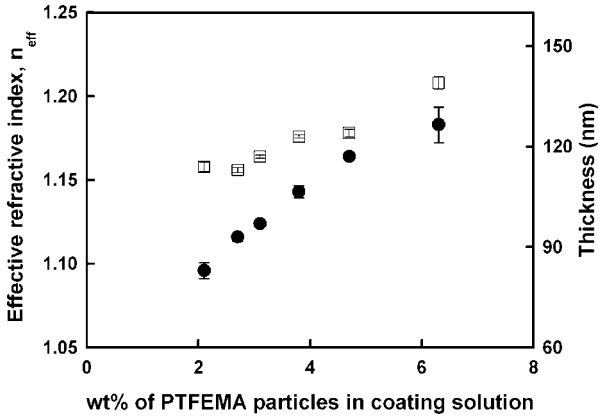


**Figure 7.** Effective refractive indices (solid circles) and coating thicknesses (open squares) estimated from the reflectance spectra of submonolayer 140 nm PTFEMA particle coatings by using eq 1.

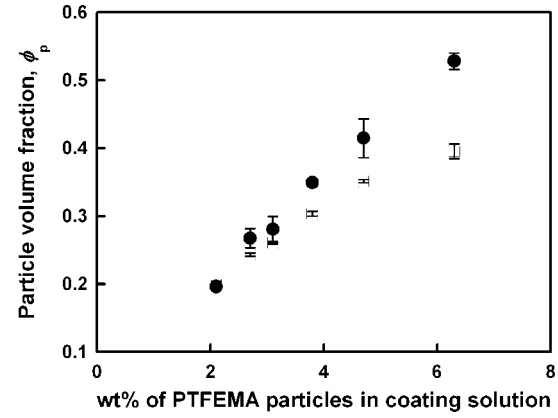


**Figure 8.** Volume fraction of particles in the submonolayer PTFEMA particle coatings determined from the effective refractive index (open squares) and from the number of particles in unit area under the assumption of monodisperse particles (solid circles).

Information). As shown in the Figure 6, measured reflectance spectra can be matched with theoretical ones accurately again. However, it must be checked whether the estimated parameters, the effective refractive index and coating thickness, are physically meaningful because the coating is discrete rather than continuous.

Figure 7 shows the effective refractive indices and thicknesses of submonolayer PTFEMA particle coatings estimated from eq 1 by fitting the measured reflectance spectra. The effective refractive index increased with the solid content of coating solutions, but less than 1.23. In that case, the minimum reflectance was inversely proportional to the effective refractive index; that is, the minimum reflectance decreased as increasing the effective reflective index contrary to the former examples where the effective refractive indices were larger than 1.23.

Another parameter deduced from the reflectance spectra is the coating thickness. As shown in Figure 7, the estimated thickness increased slightly with the surface coverage even though the same PTFEMA particles were used. In general, the thickness of submonolayer coating can be regarded as the diameter of the particle if the size of interparticle void space is subwavelength. We tried to match the measured reflectance spectrum with eq 1 by letting the film thickness as constant of the particle diameter (140 nm), but it was unsuccessful to fit the experimental results by adjusting only the effective refractive index of the coatings. One of possible explanations is the deformation of particles during the drying at ambient condition. According to the cross-sectional scanning electron microscope image for the submonolayer coating prepared from 6.3 wt % coating solution, the particles seem to be flattened (Figure S4 in Supporting Information). What is more, the coating structure starts changing from submonolayer to multilayer instead of filling unoccupied interparticle space. This observation can also explain the relatively steep increase of coating thickness when the concentration of the coating solution exceeds 6 wt % as shown in Figure 7.

The thickness control in antireflection coatings is very important when it is required that the minimum reflectance appears at desired wavelength. The zero reflectance at 550 nm, at which the human eyes perceive the best resolved color, is implemented in usual applications. Since the optimized refractive index of coating is 1.23 for glass substrate, the quarter wavelength thickness ($h_{1/4} = 0.25\lambda/n_c$) should be 112 nm. This means that slightly smaller PTFEMA particles should have been used in order that reflectance minima appeared at visible wavelengths between 500 and 600 nm. For antireflection surfaces produced from submonolayer particle coatings, the thickness can be controlled by particle size.

The information on the particle volume fraction in the coatings can be obtained from the effective refractive index by using eq 2 as described in the previous section. The maximum particle volume fraction achieved in the present study was 0.40 for submonolayer particle coatings, which was still lower than the target 0.505 for zero reflectance. In order to evaluate the validity of the estimated particle volume fraction, another method was applied separately. At first, the number of particles in unit area was calculated from the electron microscope images taken at five different places for each sample. Each image contained more than 300 particles. By assuming that the particles were monodisperse in size, the volume fraction of the particles in the coating could be estimated as given in Figure 8. The number of particles in unit area was increased almost linearly as increasing the solid content of the coating solutions (Figure S5 in Supporting Information). The maximum volume fraction of the particles calculated from this approach was about 0.52. The deviation between these two methods for estimation of particle volume fraction becomes outstanding as the surface coverage increases. It can be attributed to the polydispersity of the PTFEMA latex particles. Because of the same reason, the deviation becomes trivial as the surface coverage decreasing, where the effect of the polydispersity of the particles is less important because of the smaller number of particles in unit area. It is also anticipated that the deformability of latex particles plays some role.

In Figure 9, the reflectance minima measured at near normal incidence (5°) are illustrated for both the 47 and 140 nm PTFEMA particle coated surfaces as a function of particle volume fraction, which is determined from the effective refractive index. In addition, the solid curve stands for the theoretical reflectance minima for single-side PTFEMA particle coatings at normal incidence. It has been calculated from eq 1, by assuming quarter wavelength thickness of coating and combining with eq 2. As we can see, the measured and predicted reflectance minima are in good agreement in spite of slight difference in an incidence angle of light. It must be reminded that the wavelengths at the minimum reflectance are not identical in case of 140 nm PTFEMA particle coatings since the refractive index and thickness of the coating are increased with particle volume fraction.

In order to accomplish the zero reflectance condition, more PTFEMA particles should reside on the surface. However, unfortunately, further increasing of solid content of coating solutions resulted in transition of coating structure from submonolayer to multilayer rather than more closely packed amorphous monolayer as described before. In order to increase the packing density the particles must be pressed to each other

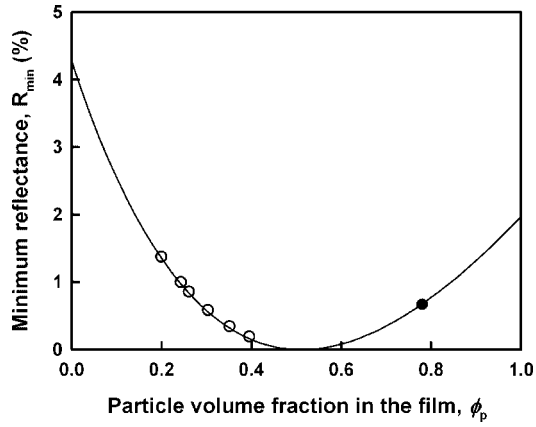


**Figure 9.** Reflectance minima measured from submonolayer coatings of 140 nm PTFEMA particles (open circles). The solid circle stands for the minimum reflectance measured from multilayer coating of 47 nm PTFEMA particles with thickness 102 nm. The theoretical reflectance minima for single-side PTFEMA coating with the quarter-wavelength thickness on glass slide at normal incidence are shown as a solid curve.

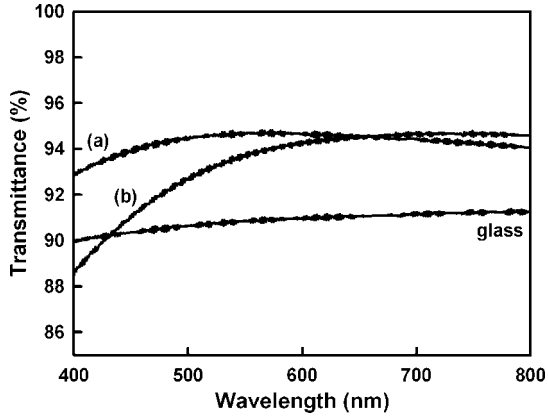


**Figure 10.** Transmittance spectra of (a) multilayer 47 nm PTFEMA particle coating prepared from 6.3 wt % coating solution and (b) submonolayer 140 nm PTFEMA particle coating from 6.3 wt % coating solution.

by external forces from a carefully maintained balance between the hydrodynamic influx and capillary forces, which is a time-consuming process.[39]

Finally, Figure 10 shows representative examples of transmittance spectra for multilayer and submonolayer PTFEMA coatings measured at normal incidence. A single side of the glass slides was spin-coated. In both cases, the light transmission is enhanced significantly. The maximum transmittance was 94.8% at 570 nm for multilayer 47 nm PTFEMA particle coating, and this means that there is little light loss resulted from scattering. By comparing reflectance spectrum shown in Figure 3b, it can be found that wavelength at maximum transmittance was not the same with that showing minimum reflectance due to the difference in incidence angle of light.

In contrast, the transmittance of submonolayer coating produced from larger PTFEMA particles was lower than expected. The maximum transmittance of submonolayer coating was almost the same with that of multilayer coating incidentally even though it showed a lower specular reflectance. Moreover, antireflection performance vanished rapidly as the wavelength of incident light decreased. This is due to the diffuse reflection of light resulting from the roughened surface with considerable length scale with incident light. However, this is not a drawback in every application. Even though the primary objective is the enhancement of light transmission in many applications of antireflection coatings, the diffuse reflection is introduced intentionally in order to reduce the glare by trading off light transmission.

Until now, we have shown that the deposition of colloidal particles is an effective and simple method to prepare antireflection surfaces with minimal processes. However, there remain several problems to be solved in order to make particle deposition of fluorinated latex particles more practicable to the antireflection coatings. For example, their poor adhesion to the substrate and durability against wear must be improved further.

## Conclusion

Transparent porous coatings with antireflective property were produced by the spin-coating of fluorinated latex particles onto the glass slides. The effective refractive index of the coatings was the most important parameter to determine the overall antireflection efficiency. For the smaller 47 nm PTFEMA particles, the solid content of the latex dispersions was varied and allowed multilayer porous films with various thicknesses. In most examples, the coatings had a random close-packed structure with the particle volume fraction around 0.80. The effective refractive indices ($n_{eff} \sim 1.34$) and reflectance minima ($R_{min} \sim 0.7\%$) were nearly constant independent of the coating thickness. The submonolayer porous coatings of the larger latex particles were also considered. As increasing the solid content of coating solutions, the surface coverage and the effective refractive indices were increased. The maximum particle volume fraction and the effective reflective index obtained in this study were 0.40 and 1.20, respectively, and the corresponding minimum reflectance was as low as 0.2%. In both cases, the large area uniformity was observed with little long-range ordering. The characteristic matrix theory based on the classical Fresnel coefficient of reflection could be successfully applied to estimate the effective refractive indices and thickness of coatings whether the film is homogeneous or porous.

**Acknowledgment.** This research was supported by a grant from the Fundamental R&D Program for Core Technology of Materials funded by the Ministry of Knowledge Economy, Republic of Korea.

**Supporting Information Available:** Reflectance spectra of PTFEMA homogeneous films, coefficients of variations of reflectance spectra for PTFEMA multilayer coating, effect of rotation speed on the antireflective efficiency during spin-coating, the number of particles in unit area for 140 nm PTFEMA submonolayer coatings, and cross-sectional SEM image of 140 nm PTFEMA coating. This material is available free of charge via the Internet at http://pubs.acs.org.

## References and Notes

(1) Born, M.; Wolf, E. *Principles of Optics*; Pergamon: New York, 1980.
(2) Macleod, H. A. *Thin-Film Optical Filters*; Macmillan Pub. Co.: New York, 1986.
(3) Ashfold, M. N. R.; Claeyssens, F.; Fuge, G. M.; Henley, S. J. *Chem. Soc. Rev.* **2004**, *33*, 23–31.
(4) Nagel, H.; Metz, A.; Hezel, R. *Sol. Energy Mater. Sol. Cells* **2001**, *65*, 71–77.
(5) Richards, B. S. *Sol. Energy Mater. Sol. Cells* **2003**, *79*, 369–390.
(6) Lee, J. H.; Cho, J. S.; Koh, S. K.; Kim, D. *Thin Solid Films* **2004**, *449*, 147–151.
(7) Xi, J.-Q.; Schubert, M. F.; Kim, J. K.; Schubert, E. F.; Chen, M.; Lin, S.-Y.; Liu, W.; Smart, J. A. *Nat. Photonics* **2007**, *1*, 176–179.
(8) Huang, J.; Wang, X.; Wang, Z. L. *Nanotechnology* **2008**, *19*, 025602.
(9) Walheim, S.; Schäffer, E.; Mlynek, J.; Steiner, U. *Science* **1999**, *283*, 520–522.
(10) Joo, W.; Park, M. S.; Kim, J. K. *Langmuir* **2006**, *22*, 7960–7963.
(11) Ballif, C.; Dicker, J.; Borchert, D.; Hofmann, T. *Sol. Energy Mater. Sol. Cells* **2004**, *82*, 331–344.
(12) Park, M. S.; Lee, Y.; Kim, J. K. *Chem. Mater.* **2005**, *17*, 3944–3950.

(13) Vincent, A.; Babu, S.; Brinley, E.; Karakoti, A.; Deshpande, S.; Seal, S. *J. Phys. Chem. C* **2007**, *111*, 8291–8298.
(14) Kim, S.; Cho, J.; Char, K. *Langmuir* **2007**, *23*, 6737–6743.
(15) Hiller, J.; Mendelsohn, J. D.; Rubner, M. F. *Nat. Mater.* **2002**, *1*, 59–63.
(16) Rouse, J. H.; Ferguson, G. S. *J. Am. Chem. Soc.* **2003**, *125*, 15529–15536.
(17) Cho, J.; Hong, J.; Char, K.; Caruso, F. *J. Am. Chem. Soc.* **2006**, *128*, 9935–9942.
(18) Lee, D.; Rubner, M. F.; Cohen, R. E. *Nano Lett.* **2006**, *6*, 2305–2312.
(19) Wu, Z.; Walish, J.; Nolte, A.; Zhai, L.; Cohen, R. E.; Rubner, M. F. *Adv. Mater.* **2006**, *18*, 2699–2702.
(20) Zhang, X.-T.; Sato, O.; Taguchi, M.; Einaga, Y.; Murakami, T.; Fujishima, A. *Chem. Mater.* **2005**, *17*, 696–700.
(21) Hattori, H. *Adv. Mater.* **2001**, *13*, 51–54.
(22) Koo, H. Y.; Yi, D. K.; Yoo, S. J.; Kim, D.-Y. *Adv. Mater.* **2004**, *16*, 274–277.
(23) Prevo, B. G.; Hwang, Y.; Velev, O. D. *Chem. Mater.* **2005**, *17*, 3642–3651.
(24) Prevo, B. G.; Kuncicky, D. M.; Velev, O. D. *Colloids Surf., A* **2007**, *311*, 2–10.
(25) Jiang, H.; Yu, K.; Wang, Y. *Opt. Lett.* **2007**, *32*, 575–577.
(26) Zhao, Y.; Wang, J.; Mao, G. *Opt. Lett.* **2005**, *30*, 1885–1887.
(27) Krogman, K. C.; Druffel, T.; Sunkara, M. K. *Nanotechnology* **2005**, *16*, S338−S343.
(28) Linn, N. C.; Sun, C.-H.; Jiang, P.; Jiang, B. *Appl. Phys. Lett.* **2007**, *91*, 101108.
(29) Sun, C.-H.; Min, W.-L.; Linn, N. C.; Jiang, P.; Jiang, B. *Appl. Phys. Lett.* **2007**, *91*, 231105.
(30) Sun, C.-H.; Gonzalez, A.; Linn, N. C.; Jiang, P.; Jiang, B. *Appl. Phys. Lett.* **2008**, *92*, 051107.
(31) Scheirs, J. *Modern Fluoropolymers*; Wiley: New York, 1997.
(32) Hougham, G.; Davidson, T.; Cassidy, P.; Johns, K. *Fluoropolymers*; Plenum: New York, 1999.
(33) Ameduri, B.; Boutevin, B. *Well-Architectured Fluoropolymers: Synthesis, Properties and Applications*; Elsevier: Amsterdam, 2004.
(34) Yoldas, B. E. *Appl. Opt.* **1980**, *19*, 1425–1429.
(35) Braun, M. M.; Pilon, L. *Thin Solid Films* **2006**, *496*, 505–514.
(36) Pansu, B.; Pieranski, P.; Strzelecki, L. *J. Phys. (Paris)* **1983**, *44*, 531–536.
(37) Pansu, B.; Pieranski, Pi.; Pieranski, Pa. *J. Phys. (Paris)* **1984**, *45*, 331–339.
(38) Prevo, B. G.; Velev, O. D. *Langmuir* **2004**, *20*, 2099–2107.
(39) Dimitrov, A. S.; Miwa, T.; Nagayama, K. *Langmuir* **1999**, *15*, 5257–5264.

MA801224W